Metallosupramolecular Equilibria



# Monitoring Metallo-Macromolecular Assembly Equilibria by Ion Mobility-Mass Spectrometry

Kevin J. Endres, Ting-Zheng Xie, Sourav Chakraborty, Chad Hoopingarner, and Chrys Wesdemiotis\*

Dedicated to Professor George R. Newkome on the occasion of his 80th birthday and for his innumerous seminal contributions to the fields of dendrimers and coordination chemistry.

Ion mobility-mass spectrometry (IM-MS) allows the separation of isomeric and isobaric species on the basis of their size, shape, and charge. The fast separation timescale (ms) and high sensitivity of these measurements make IM-MS an ideally suitable method for monitoring changes in macromolecular structure, such as those occurring in interconverting terpyridine-based metallosupramolecular self-assemblies. IM-MS is used to verify the elemental composition (size) and architecture (shape) of the self-assembled products. Additionally, this article demonstrates its applicability to the elucidation of concentration-driven association-dissociation (fusion-fission) equilibria between isobaric structures. IM-MS enables both quantitative separation and identification of the interconverting complexes as well as derivation of the corresponding equilibrium constants (i.e., thermodynamic information) from extracted IM-MS abundance data.

Macromolecular association is widespread in biology, where chemical reactions occur mostly within multicomponent complexes.[1] For example, many proteins form higher-order assemblies in order to carry out enzymatic function, [2-4] as is evident from the large number of multimeric proteins in the Protein Data Bank.<sup>[5]</sup> Protein (and other biomolecule) multimers are normally formed by reversible subunit association, triggered by concentration, pH, or ionic strength changes. [6-9] The latter factors may also promote abnormal, irreversible aggregation which is believed to be the cause of several neurodegenerative disorders.[10] Mass spectrometry (MS) using electrospray ionization (ESI) has played a key role in the elucidation of biomolecular association-dissociation equilibria and the composition and structure of the complexes arising in such reactions.[11,12] As a soft ionization method, ESI ensures that higher-order structures are gently transferred from solution to the gas phase in the mass spectrometer, which then probes the mass-to-charge ratios (m/z) of the detected components to reveal the multimer state(s) and/or dissociation product(s) formed.

ESI-MS analyses of macromolecular aggregates are substantially facilitated by interfacing mass analysis (i.e., m/z measurement) with ion mobility (IM) separation.[11-17] In an ion mobility-mass spectrometry (IM-MS) experiment, ions drift through a bath gas under the influence of an electric field and are dispersed in this event according to their collision crosssection (CCS) and charge.[16,18-20] CCS is

the rotationally averaged forward-moving area of the ion and depends both on its size and shape. Ions in low charge states travel more slowly through the IM region than more highly charged ions. Similarly, ions with larger CCS undergo more collisions with the bath gas in the IM region and, hence, move more slowly through it than ions with smaller CCS. These features allow separation of coexisting isomers and conformers (which have the same m/z) as well as coexisting isobars (which have very similar m/z values and overlapping isotope patterns), provided there are differences in charge state or CCS. Separation through the IM dimension followed by mass analysis of the separated species yields a drift time distribution or "mobilogram" which, in analogy to a chromatogram, reveals whether isomerizations, conformational changes, or oligomerizations have taken place based on the number of peaks observed.[14-26] For each species observed in the mobilogram, an experimental CCS can be deduced from the corresponding drift time.[16,19] Comparison of this CCS with modeled CCS values for specific structures and geometries permits precise identification of the connectivities and 3D structures of the isolated species.<sup>[22]</sup>

Macromolecular association or aggregation can also occur in solutions of abiotic systems that are able to rearrange between monomeric and multimeric forms. Supramolecular polymers are prone to undergo such interconversions, as they are held together through noncovalent or metal-ligand interactions that are easier to break and reform than the  $\sigma$  or  $\pi$  bonds in

K. J. Endres, Dr. T.-Z. Xie, Dr. S. Chakraborty, C. Hoopingarner Department of Polymer Science The University of Akron Akron, OH 44325, USA Prof. C. Wesdemiotis Departments of Chemistry and Polymer Science The University of Akron

Akron, OH 44325, USA

E-mail: wesdemiotis@uakron.edu

The ORCID identification number(s) for the author(s) of this article can be found under https://doi.org/10.1002/marc.201800667.

DOI: 10.1002/marc.201800667

covalently bonded polymers.<sup>[27-30]</sup> These polymers can dissociate or associate when exposed to external stimuli, like a change in temperature, concentration, pH, or solvent, which makes them ideally suitable for the generation of "smart" functional materials that can be tuned for drug delivery, molecular recognition, catalysis, and other biomedical or engineering applications.<sup>[27-30]</sup> A promising and widely investigated class of supramolecular polymers with such properties are terpyridine-based coordination complexes.<sup>[29-31]</sup>

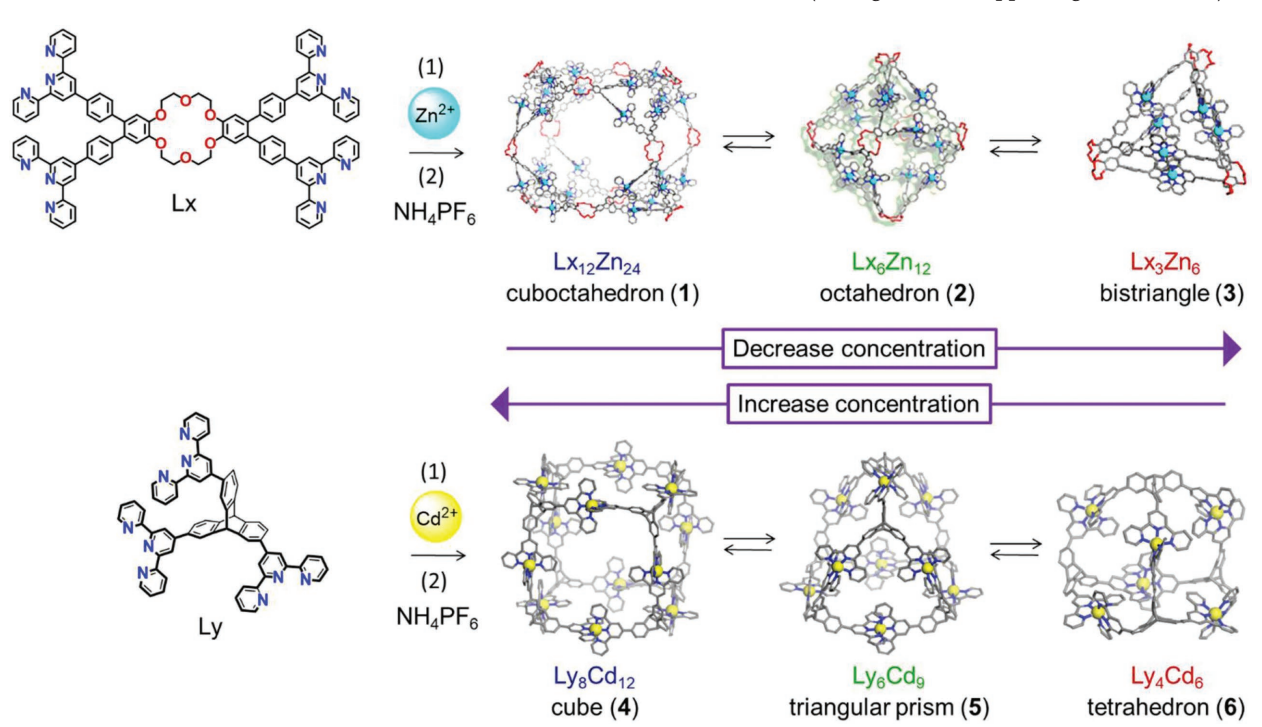
The coordinatively driven self-assembly of terpyridine ligands with transition metal ions proceeds via kinetic control, leading to one or more stable constructs, or via thermodynamically controlled reversible equilibria, creating labile and interconvertible complexes;<sup>[30,31]</sup> in either case, overlapping isobars, isomers, and/or conformers are possible. Since liquid chromatography (LC) is often inapplicable to organometallic complexes, using IM-MS is instrumental for the separation of the overlapping species by the IM dimension, so that their molecular compositions can be ascertained with confidence in the orthogonal MS dimension. [32,33] Moreover, the IM step also reveals the CCS values of the examined complexes which are an important physical parameter diagnostic of their size and architecture (vide supra).

Several new terpyridine-based assemblies with the connectivity <tpy-M<sup>2+</sup>-tpy> (tpy, terpyridine; M, transition metal ion) have been discovered and conclusively characterized by ESI-IM-MS, including a highly symmetric nanosphere,<sup>[33–35]</sup> 3D molecular wheels,<sup>[36,37]</sup> cuboctahedra,<sup>[38,39]</sup> and isomeric nanocages.<sup>[35]</sup> In addition, reversible association–dissociation (fusion–fission) equilibria in supramolecules with weak Cd<sup>2+</sup>-tpy and Zn<sup>2+</sup>-tpy bonds could be observed by ESI-IM-MS upon changing concentration or the counterion.<sup>[35,37–41]</sup>

In spite of this progress, it has remained challenging to measure the equilibrium constants of the aforementioned processes. Select association constants between tpy and M<sup>2+</sup> have been assessed qualitatively and quantitatively by single-stage mass spectrometry<sup>[42]</sup> and isothermal titration calorimetry,<sup>[43]</sup> respectively. Architectural changes and the effect of counterions were not considered in these studies.

This article illustrates how ESI-IM-MS can be utilized to elucidate architectural changes and fission–fusion interconversions during the self-assembly of Zn²+ cations with tetrakisterpyridinyl ligands substituted by 18-crown-6,<sup>[39]</sup> and Cd²+ cations with tris-terpyridinyl spiral ligands.<sup>[41]</sup> IM-MS is employed to separate the isobaric macromolecules produced from solutions in equilibrium over a range of metal/ligand concentrations. Quantitative analysis of the isobaric architectures generated in fission–fusion equilibria based on extracted mobilogram peak areas is demonstrated for the first time. Additionally, a protocol for calculating equilibrium constants from the extracted mobilograms is detailed.

The angles between the metal binding sites in ligands Lx and Ly were designed to promote self-assembly to the large complexes 1 and 4, respectively (Scheme 1). Indeed, analysis of the isolated solid products (by X-ray diffraction) and their concentrated solutions (by ESI-MS or NMR spectroscopy) confirms that these large complexes have been formed (cf. Figure S1, Supporting Information). As the analyzed solutions are increasingly diluted, the large complexes 1 and 4 gradually rearrange to the smaller constructs 2 and 5, respectively, and further dilution gives rise to the even smaller complexes 3 and 6, respectively, which dominate at the smallest possible detectable concentrations (cf. Figure S2, Supporting Information). Such



**Scheme 1.** Self-assembly of a) ligand Lx with  $Zn^{2+}$  ions mixed in the exact stoichiometric ratio 1:2 and b) ligand Ly with  $Cd^{2+}$  ions mixed in the exact stoichiometric ratio 2:3. The complexes formed were isolated as  $PF_6^-$  salts, dried, and re-dissolved at different concentrations, which is equivalent to using different initial concentrations of the ligands and metal ions.

supramolecular interconversions attest the occurrence of concentration-dependent, dynamic fission–fusion equilibria, made possible by the flexible geometry of ligands Lx and Ly and the lability of <tpy-M<sup>2+</sup>-tpy> (M = Zn or Cd) coordinative bonds. These interconversions are detectable and characterizable by NMR or UV–vis spectroscopy, if each species in the mixture exhibits unique resonances; unfortunately, this condition is rarely fulfilled with hierarchical multicomponent mixtures containing the same ligand and metal.

It is worth noting that the monodisperse products present at the highest and at lower concentrations produce a series of peaks upon ESI-MS, depending on the number of  $PF_6^-$  counterions lost (Figures S1 and S2, Supporting Information). Intermediate concentrations expectedly lead to mixtures with complex spectral characteristics, as illustrated in **Figure 1**, where some of the peaks observed are unique to a certain complex, while other peaks may contain superimposed ions of two or three complexes. For example, the peak at m/z 1235.21 (Figure 1a) includes contributions from cuboctahedron 1 (loss of 20  $PF_6^-$  counterions), octahedron 2 (loss of 10  $PF_6^-$  counterions), and bistriangle 3 (loss of 5  $PF_6^-$  counterions); these species have 20+, 10+, and 5+ charges, respectively, and all overlap at m/z 1235.21. Their different sizes and charges permit, however, separation by the corresponding ion mobilities.

Overlapping species within the same m/z ratio can be resolved if they are sent through the IM region. This is illustrated in Figure 1b for complexes with ligand Lx superimposed at m/z 2155.55 and in Figure 1d for complexes with ligand Ly superimposed at m/z 1406.65. In both cases, the IM-MS

mobilograms indicate the presence of three species. The three self-assembly products of Lx and Zn<sup>2+</sup>, viz. cuboctahedron 1, octahedron 2, and bistriangle 3, are observed at drift times of 7.13, 9.39, and 14.17 ms, respectively (Figure 1b). Conversely, the three self-assembly products of Ly and Cd<sup>2+</sup>, viz. cube 4, triangular prism 5, and tetrahedron 6, are observed at 4.06, 5.85, and 6.50 ms, respectively. These assignments were made based on the drift times of m/z 2155.55 and 1406.65 at high (Figure S1, Supporting Information) or low (Figure S2, Supporting Information) concentration, at which monodisperse complexes with a single drift time are observed, and based on the isotope pattern of the mass spectra extracted from the mobilograms (cf. Figure S3, Supporting Information).

Table S1 and Figure S4, Supporting Information summarize the CCS of the equilibrating assemblies 1-3 and 4-6, derived from the drift times observed in ESI-IM-MS mobilograms. CCS generally increases with mass, but also depends on the geometry of the ligands and the final self-assemblies. It is noteworthy that a significantly larger conformational space is sampled by  $1 \rightarrow 2 \rightarrow 3$  than by  $4 \rightarrow 5 \rightarrow 6$  (786–2432 vs 778–1249 Å<sup>2</sup>, respectively), due to the flexibility of crown-ether containing ligand Lx. For the largest complex examined, viz. cuboctahedron 1, three different conformers are observed depending on the number of counterions remaining after ESI.<sup>[39]</sup> As the number of PF<sub>6</sub><sup>-</sup> counterions increases, charge repulsions between the Zn<sup>2+</sup> centers are mitigated, causing contraction of the cuboctahedron self-assembly (cf. Figure S4, Supporting Information). Such structural changes can potentially be exploited for encapsulation and release of proper guests and for sensing applications.

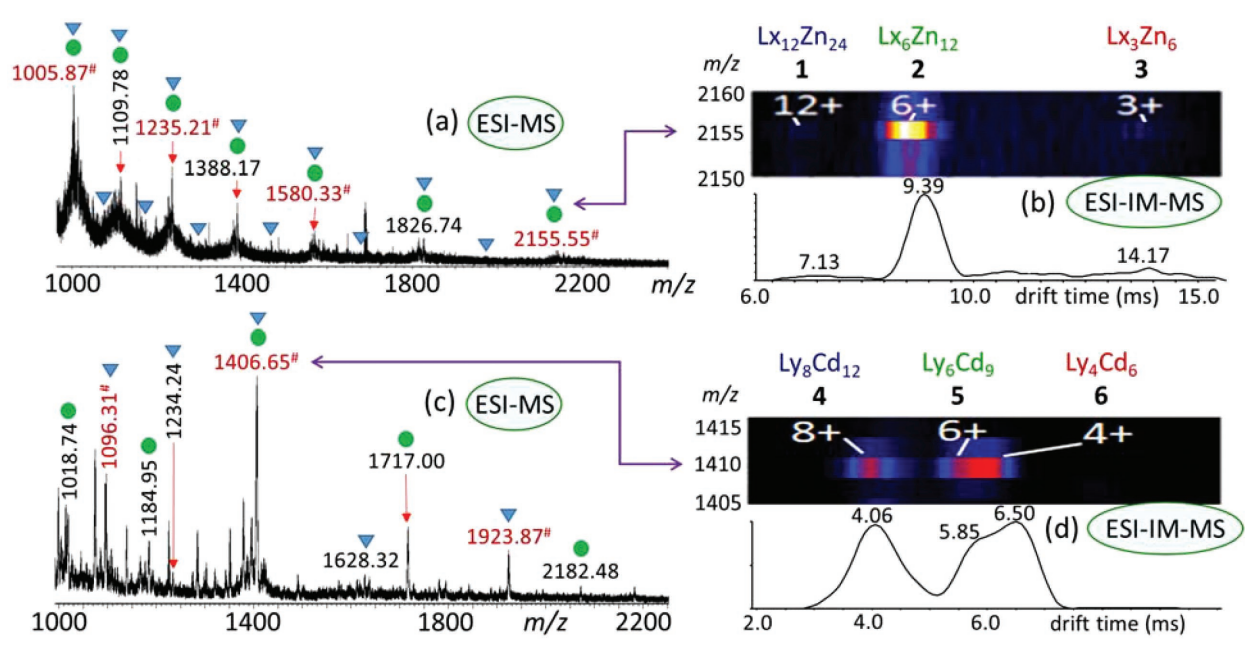


Figure 1. a) ESI-MS spectrum of a mixture of cuboctahedron 1 ( $Lx_{12}Zn_{24}$ ) (blue triangles), octahedron 2 ( $Lx_6Zn_{12}$ ) (green circles), and bistriangle 3 ( $Lx_3Zn_6$ ) (red # labeled peaks), acquired from a 0.20 mg mL<sup>-1</sup> solution of isolated solid  $Lx_{12}Zn_{24}(PF_6)_{48}$ . b) ESI-IM-MS mobilogram of m/z 2155.55 shown as 2D plot (top) and drift time distribution (bottom); the IM dimension separates  $Lx_{12}Zn_{24}^{12+}$  (1 with 36 PF $_6$ -counterions),  $Lx_6Zn_{12}^{6+}$  (2 with 18 PF $_6$ -counterions), and  $Lx_3Zn_6^{3+}$  (3 with 9 PF $_6$ -counterions), all of which overlap at m/z 2155.55. c) ESI-MS spectrum of a mixture of cube 4 ( $Ly_8Cd_{12}$ ) (blue triangles), triangular prism 5 ( $Ly_6Cd_9$ ) (green circles), and tetrahedron 6 ( $Ly_4Cd_6$ ) (red # labeled peaks), acquired from a 0.40 mg mL<sup>-1</sup> solution of isolated solid  $Ly_3Cd_{12}(PF_6)_{24}$ . d) ESI-IM-MS mobilogram of m/z 1406.65 shown as 2D plot (top) and drift time distribution (bottom); the IM dimension separates  $Lx_3Cd_{12}^{8+}$  (4 with 16 PF $_6$ -counterions),  $Ly_6Cd_9^{6+}$  (5 with 12 PF $_6$ -counterions), and  $Ly_4Cd_6^{4+}$  (6 with 8 PF $_6$ -counterions), all of which overlap at m/z 1406.65.

The cuboctahedron species detected at 7.13 ms in Figure 1b corresponds to the most compact conformer (36  ${\rm PF_6}^-$  counterions). This structure should predominate in the polar solvents used to dissolve the isolated self-assembly (ACN and DMSO), in which like-charge repulsions can be stabilized by solvation. Hence, this compact conformer was considered in the evaluation of supramolecular equilibria and equilibrium constants (vide infra).

The interconversions  $1 \rightleftharpoons 2 \rightleftharpoons 3$  and  $4 \rightleftharpoons 5 \rightleftharpoons 6$  were monitored by ESI-IM-MS analysis of solutions made from the isolated solids over the concentration ranges 1.00–0.02 mg mL<sup>-1</sup> and 10.0–0.05 mg mL<sup>-1</sup>, respectively (see Experimental Section). At each concentration, the intensities (peak areas) of the three components of m/z 2155.55 from the Lx/Zn<sup>2+</sup> complexes and the three components of m/z 1406.65 from the Ly/Cd<sup>2+</sup> complexes were measured and the relative proportion (%) of each structure was plotted as a function of concentration, cf. **Figure 2**.

The peaks at m/z 2155.55 and 1406.65 were selected for probing the dependence of solution composition on concentration because all three isobaric structures of the Lx/Zn<sup>2+</sup> and Ly/Cd<sup>2+</sup> complexes produce ions of these m/z ratios, respectively. Moreover, these peaks were reasonably abundant over the sampled concentration range and their isobaric components were satisfactorily resolved in the IM dimension. More importantly, monitoring a single m/z for all three interconverting species eliminated discrepancies in ionization, transmission, and detection efficiency, since signal intensity is dependent on ion velocity which is practically constant for isobaric ions. [44,45]

The actual intensity data extracted from the ESI-IM-MS mobilograms in order to plot Figure 2 are listed in Tables S2, S3, Supporting Information, together with the corresponding standard deviations from triplicate measurements, which are indicated by error bars in Figure 2. It is evident that reproducibility is poorer at lower concentrations as a result of the lower total ion counts (TICs) detected at high dilution. Nonetheless, the relative amount of each structure is traced properly despite the lower sensitivity at the low concentrations.

The plots in Figure 2 demonstrate that ligand complexation with either divalent Zn or Cd metal ions is a dynamic process occurring over a concentration range that is ligand dependent. Significant and very similar interconversions are observed when concentration is varied within ca. 1–200  $\mu$ m for the Lx/Zn<sup>2+</sup> self-assemblies and within ca. 5–2000  $\mu$ m for the Ly/Cd<sup>2+</sup> self-assemblies. Equilibrium between the largest structure (cuboctahedron 1

or cube 4) and the middle structure (octahedron 2 or triangular prism 5, respectively) is observed over a wide concentration range for both equilibria in Scheme 1. These structures are readily monitored because they exist in the typical concentration range infused into the ESI source (0.10–1.00 mg mL<sup>-1</sup>). More concentrated solutions of such structures (>1.00 mg mL<sup>-1</sup>) tend to contaminate the ESI source; therefore, solutions were analyzed in order of increasing concentration and the ion source was thoroughly cleaned between infusions in order to avoid memory effects from residual sample not cleaned out.

For a more quantitative assessment of the supramolecular interconversions taking place in the analyzed solutions, equilibrium constants were derived for the isomerization of each complex to a mixture of the other two complexes, as shown in Equations (1)–(6). Since ligand and metal were mixed in precise stoichiometric ratios (see Experimental Section), both were assumed to have reacted completely in the initial self-assembly reaction. Therefore, the equilibria examined include solely the three interconverting constructs (cf. Equations (1a)–(6a)). Counterions and charge states have been omitted from these equations for brevity.

$$Lx_{12}Zn_{24}(1) \rightleftharpoons 2Lx_3Zn_6(3) + Lx_6Zn_{12}(2)$$
 (1a)

$$K_1 = \frac{[Lx_3Zn_6]^2[Lx_6Zn_{12}]}{[Lx_{12}Zn_{24}]} = 2.6 \times 10^{-11} \quad (pK_1 = 10.21)$$
 (1b)

$$3Lx_6Zn_{12}(2) \rightleftharpoons 2Lx_3Zn_6(3) + Lx_{12}Zn_{24}(1)$$
 (2a)

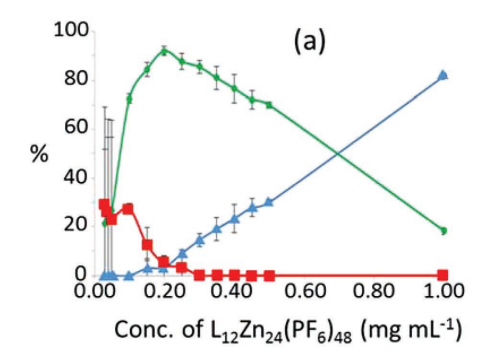
$$K_2 = \frac{[\text{Lx}_3 \text{Z} \text{n}_6]^2 [\text{Lx}_{12} \text{Z} \text{n}_{24}]}{[\text{Lx}_6 \text{Z} \text{n}_{12}]^3} = 3.4 \times 10^{-4} \quad (\text{pK}_2 = 3.66)$$
 (2b)

$$6Lx_3Zn_6(3) \rightleftharpoons Lx_{12}Zn_{24}(1) + Lx_6Zn_{12}(2)$$
(3a)

$$K_3 = \frac{[Lx_{12}Zn_{24}][Lx_6Zn_{12}]}{[Lx_3Zn_6]^6} = 2.6 \times 10^{26} \quad (pK_3 = -25.40)$$
 (3b)

$$2 \operatorname{Ly}_{8} \operatorname{Cd}_{12}(\mathbf{4}) \rightleftharpoons \operatorname{Ly}_{4} \operatorname{Cd}_{6}(\mathbf{6}) + 2 \operatorname{Ly}_{6} \operatorname{Cd}_{9}(\mathbf{5}) \tag{4a}$$

$$K_4 = \frac{[Ly_4Cd_6][Ly_6Cd_9]^2}{[Ly_8Cd_{12}]^2} = 1.2 \times 10^{-5} \quad (pK_4 = 5.03)$$
 (4b)



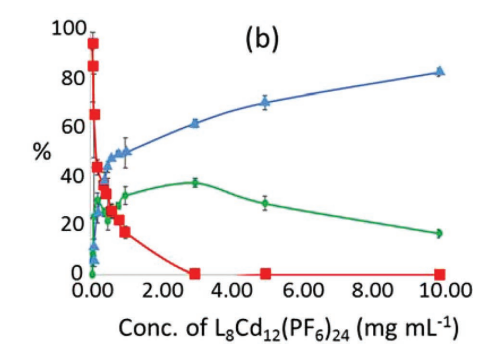


Figure 2. Plots displaying the relative abundances of a) bistriangle  $Lx_3Zn_6^{3+}$  (red squares), octahedron  $Lx_6Zn_{12}^{6+}$  (green circles), and cuboctahedron  $Lx_{12}Zn_{24}^{12+}$  (blue triangles) over a range of  $Lx_{12}Zn_{24}(PF_6)_{48}$  concentrations and b) tetrahedron  $Ly_4Cd_6^{4+}$  (red squares), triangular prism  $Ly_6Cd_9^{6+}$  (green circles), and cube  $Ly_8Cd_{12}^{8+}$  (blue triangles) over a range of  $Ly_8Cd_{12}(PF_6)_{24}$  concentrations.

www.advancedsciencenews.com

$$2 \operatorname{Ly}_{6} \operatorname{Cd}_{9}(\mathbf{5}) \rightleftharpoons \operatorname{Ly}_{8} \operatorname{Cd}_{12}(\mathbf{4}) + \operatorname{Ly}_{4} \operatorname{Cd}_{6}(\mathbf{6})$$
 (5a)

$$K_5 = \frac{[Ly_8Cd_{12}][Ly_4Cd_6]}{[Ly_6Cd_9]^2} = 2.4 \times 10^0 \quad (pK_5 = -0.27)$$
 (5b)

$$5 \operatorname{Ly}_{4}\operatorname{Cd}_{6}(\mathbf{6}) \rightleftharpoons \operatorname{Ly}_{8}\operatorname{Cd}_{12}(\mathbf{4}) + 2 \operatorname{Ly}_{6}\operatorname{Cd}_{9}(\mathbf{5}) \tag{6a}$$

$$K_6 = \frac{[Ly_8Cd_{12}][Ly_6Cd_9]^2}{[Ly_4Cd_6]^5} = 7.8 \times 10^9 \quad (pK_6 = -9.25)$$
 (6b)

Reactions 1a and 4a involve dissociation of cuboctahedron 1 or cube 4 to smaller complexes, whereas the other reactions correspond to association processes that generate one of these largest possible products. These equilibria sample all three architectures of the Lx/Zn<sup>2+</sup> and Ly/Cd<sup>2+</sup> complexes which coexist in the low to medium concentration range (cf. Figure 2). The largest Lx/Zn<sup>2+</sup> self-assembly (i.e., cuboctahedron 1) is not observed at very low concentration; conversely, the smallest Lx/Zn<sup>2+</sup> and Ly/Cd<sup>2+</sup> complexes (3 and 6, respectively) are not observed at higher concentrations (cf. Figure 2 and Tables S2, S3, Supporting Information). Therefore, equilibria involving only two constructs were also investigated; specifically, the dissociation of medium-sized octahedron 2 to the smaller bistriangle 3 which dominates at very low concentration (Equation (7)), as well as the dissociation of cuboctahedron 1 and cube 2 to medium-sized octahedron 2 and triangular prism 5, respectively, which are exclusively sampled in the higher concentration regime (Equations (8), (9)).

$$\operatorname{Lx}_{6}\operatorname{Zn}_{6}(\mathbf{2}) \rightleftharpoons 2\operatorname{Lx}_{3}\operatorname{Zn}_{6}(\mathbf{3})$$
 (7a)

$$K_{d2} = \frac{[Lx_3Zn_6]^2}{[Lx_6Zn_{12}]} = 1.9 \times 10^{-6} \quad (pK_{d2} = 5.76)$$
 (7b)

$$Lx_{12}Zn_{24}(\mathbf{1}) \rightleftharpoons 2Lx_6Zn_{12}(\mathbf{2})$$
 (8a)

$$K_{d3} = \frac{[Lx_6Zn_{12}]^2}{[Lx_1Zn_{24}]} = 5.4 \times 10^{-5} \quad (pK_{d3} = 4.47)$$
 (8b)

$$3 \operatorname{Ly}_{8} \operatorname{Cd}_{12}(4) \rightleftharpoons 4 \operatorname{Ly}_{6} \operatorname{Cd}_{9}(5) \tag{9a}$$

$$K_{d5} = \frac{[Ly_6 Cd_9]^4}{[Ly_8 Cd_{12}]^3} = 1.1 \times 10^{-5} \quad (pK_{d5} = 5.20)$$
 (9b)

The equilibrium constants for the dissociation of octahedron 2 to bistriangle 3 (Equation (7a)), cuboctahedron 1 to octahedron 2 (Equation (8a)), and cube 4 to triangular prism 5 (Equation (9a)), which interconvert two different complexes, have been termed  $K_{d2}$ ,  $K_{d3}$ , and  $K_{d5}$  respectively, to distinguish them from those involving three different complexes, viz.,  $1 \rightarrow 2 + 3$  (Equation (1a);  $K_{d1} = K_1$ ) and  $4 \rightarrow 5 + 6$  (Equation (4a);  $K_{d4} = K_4$ ).

The normalized areas of the mobility-separated peaks (cf. Figure 1) represent the mol% of 1-3 (Lx/Zn<sup>2+</sup> complexes)

or 4-6 (Ly/Cd<sup>2+</sup> complexes) in the corresponding equilibrating mixtures. These were converted to weight%, then to mg mL<sup>-1</sup>, and finally to molar concentrations (mol L-1), as described in Tables S4–S8, Supporting Information). The molarities (mol L<sup>-1</sup>) obtained this way were used to derive equilibrium constants for the supramolecular interconversions 1a-9a at ambient temperature (20 °C), which are provided in Equations (1b)–(9b), respectively. The values given are the average constants over the concentration range probed for each equilibrium (cf. Tables S9, S10, Supporting Information). Concentration changes can shift the equilibrium position, but do not affect equilibrium constants. The slight variability in the constants calculated at different concentrations is attributed to solution temperature and ion intensity fluctuations during the IM-MS measurements. It is noteworthy that these fluctuations are very small compared to the differences observed between the equilibrium constants of reactions 1a-9a, which is also clearly evident from the corresponding pK values included in Equations (1b)-(9b) and Tables S9, S10, Supporting Information.

It is worth noting at this point that the derivation of equilibrium concentrations from relative IM-MS abundances presupposes that a change in relative IM-MS abundance of a species participating in an equilibrium is caused by a change in its relative amount due to interconversion. This prerequisite was confirmed by the analysis of a supramolecular standard comprising three isobaric complexes that are kinetically stable and do not equilibrate (cf. Scheme S1 and Figures S5–S7, Supporting Information). Unlike the trends observed for complexes 1–3 and 4–6 (Figure 2), the relative amounts of the three complexes in the standard were independent of solution concentration and remained constant over the probed concentration range (cf. Figure S7, Supporting Information).

The order  $K_1 < K_2 \ll K_3$  for complexes 1–3 indicates that the formation of larger constructs with the tetrakis-terpyridinyl ligand Lx is thermodynamically favored. The order  $K_4 < K_5 < K_6$ for complexes 4–6 further corroborates that the tris-terpyridinyl ligand Ly follows the same trend. Based on the absolute values of constants  $K_1$  versus  $K_4$ ,  $K_2$  versus  $K_5$ , and  $K_3$  versus  $K_6$ , which describe equilibria that sample all three Lx or Ly complexes, there is lower proclivity to form larger self-assemblies with Ly and Cd2+ ions than with Lx and Zn2+ ions. This result reflects the lower stability of Cd<sup>2+</sup>-tpy compared to Zn<sup>2+</sup>-tpy coordinative bonds as well as the lower strain associated with smaller complexes with the Ly vis à vis the Lx ligand. The large value of K<sub>3</sub> justifies the difficulty of observing the bistriangle architecture 3 in solutions with an initial concentration >0.25 mg mL<sup>-1</sup> (cf. Table S2, Supporting Information); considerable dilution is needed to drive the position of equilibrium 3a toward the side with more molecules and form measurable quantities of this strained structure.

The dissociation constants of the binary equilibria studied, viz.  $K_{d2}$  (2  $\rightarrow$  3),  $K_{d3}$  (1  $\rightarrow$  2), and  $K_{d5}$  (4  $\rightarrow$  5), are fairly similar, all lying within the  $\mu$ M range (cf. Equations (7)–(9), respectively, and Tables S9, S10, Supporting Information). The order  $K_{d2} < K_{d3}$  reaffirms the low tendency of forming the strained bistriangle (3) architecture. This finding is further underscored by the significantly smaller constant for the dissociation of cuboctahedron 1 to a mixture of octahedron 2 plus bistriangle 3 (Equation (1);  $K_{d1} = K_1$ ) than its dissociation to just



www.advancedsciencenews.com



**2** (Equation (8);  $K_{d3}$ ). In contrast, the dissociation constants of cube **4** to either a mixture of triangular prism **5** plus tetrahedron **6** (Equation (1);  $K_{d4} = K_4$ ) or to just **5** (Equation (9);  $K_{d5}$ ) are comparable.

In summary, this study has shown that ESI-IM-MS affords an appropriate analytical tool for the comprehensive characterization of coordinatively bound supramolecules and their fusion–fission equilibria: ESI ensures the gentle transfer of the sample from solution to the gas phase, the IM dimension separates the complexes by architecture and charge, and the MS dimension establishes stoichiometry and elemental composition of the separated components. Additionally, this article introduced a new ESI-IM-MS protocol for the quantitative analysis of interconverting, superimposed complexes which permits to monitor fusion–fission equilibria and derive the corresponding equilibrium constants from extracted IM-MS mobilograms.

Fission-fusion structural changes, analogous to those taking place with proteins and other biological macromolecules, were detected and thoroughly investigated as a function of concentration for the thermodynamically controlled self-assembly of tris-pyridinyl spiral ligands (Ly) with Cd2+ cations and tetrakisterpyridinyl ligands containing an 18-crown-6 moiety (Lx) with Zn<sup>2+</sup> cations. Cd<sup>2+</sup> or Zn<sup>2+</sup> ions form relatively labile coordination bonds during self-assembly, thus generating complexes that are able to reversibly interconvert. The protocol described enabled the determination of equilibrium constants for the interconversions of coordinatively bound terpyridine-based macromolecules, thus unveiling important thermodynamic information about the stabilities of the equilibrating structures. For the specific self-assemblies examined, the measured equilibrium constants indicate increasing thermodynamic stability with increasing size of the complex, viz. in the order bistriangle << octahedron < cuboctahedron. A similar trend is found for the tris-pyridinyl-based fusion-fission equilibria where again thermodynamic stability increases with the size, viz. in the order tetrahedron < triangular prism < cube.

## **Experimental Section**

Materials: The chemicals and solvents used for the preparation of the self-assembled complexes and the mass spectrometry experiments were purchased from Sigma-Aldrich (St. Louis, MO) or Fisher Scientific (Pittsburgh, PA) and used without further purification.

Synthesis and Dilutions of Cuboctahedron (1), Octahedron (2), Bistriangle (3): The tetrakis-terpyridinyl ligand containing a central 18-crown-6 moiety, Lx (cf. Scheme 1), was synthesized as reported previously. [39] Its self-assembly with Zn²+ ions was promoted by adding a solution of Zn(NO<sub>3</sub>)<sub>2</sub>·6H<sub>2</sub>O (16 µmol) in MeOH (1 mL) to a stirred solution of Lx (8 µmol) in CHCl<sub>3</sub> and MeOH (1:1, 16 mL). After the reaction mixture was stirred for 2 h at 25 °C, a tenfold excess NH<sub>4</sub>PF<sub>6</sub> was added. The residue was filtered, washed with water and MeOH, and dried under vacuum to give cuboctahedron 1. Solid 1 was initially dissolved in DMSO (11.11 mg mL⁻¹) and then diluted with ACN (1 mg mL⁻¹ in ACN:DMSO (10.1:1 v/v). This solution was diluted further with ACN:DMSO (10.1:1 v/v) to reach concentrations below 1 mg mL⁻¹ in this solvent.

Synthesis and Dilutions of Cube (4), Triangular Prism (5), Tetrahedron (6): The tris-pyridinyl spiral ligand Ly (cf. Scheme 1) was synthesized according to a previously reported procedure. The one-step self-assembly of ligand Ly with  $Cd(NO_3)_2$ , which were combined in precise 2:3 molar ratio in stirred CHCl<sub>3</sub> and MeOH (1:1, v/v) solvent at 25 °C for 1 h, led to a

colorless solution. Counterion exchange by subsequent treatment with excess aqueous  $\rm NH_4PF_6$  solution (to exchange  $\rm NO_3^-$  for  $\rm PF_6^-$ ), followed by filtration of the precipitated solid, washing with methanol, and solvent evaporation under vacuum gave the desired complex 4. Cube 4 was dissolved in ACN, and then diluted with ACN (10 mg mL $^{-1}$ ). This solution was diluted further with ACN to reach concentrations below 10 mg mL $^{-1}$ .

Ion Mobility-Mass Spectrometry: The ESI-IM-MS experiments were performed on a Waters Synapt G1 quadrupole/time-of-flight (Q/ToF) mass spectrometer equipped with ESI and a triwave device between the Q and ToF analyzers, which comprises three collision cells in the order of trap cell, ion mobility cell, and transfer cell and is the location of IM separations.[32-41] Trap and transfer cells were pressurized with Ar, and the ion mobility cell was pressurized with N2 flowing in a direction opposite to that of the entering ions. All samples were analyzed in triplicate using the following parameters: ESI capillary voltage, 2 kV; sample cone voltage, 35 V; extraction cone voltage, 3.2 V; desolvation gas flow, 500 L  $h^{-1}$  ( $N_2$ ); trap cell collision energy (CE), 6 eV; transfer cell CE, 4 eV; trap/transfer gas flow, 1.5 mL min<sup>-1</sup> (Ar); ion mobility cell gas flow, 22.7 mL min<sup>-1</sup> (N<sub>2</sub>); sample flow rate, 5  $\mu$ L min<sup>-1</sup>; source temperature, 80 °C; desolvation temperature, 150 °C; traveling-wave height, 7.5 V; and traveling-wave velocity, 350 m s<sup>-1</sup>. Data analyses were conducted using the MassLynx 4.1 and DriftScope 2.8 programs provided by Waters.

IM separation resolves overlapping isobaric ions which were mass analyzed by the ToF analyzer after exiting the IM cell. A mobilogram was obtained by plotting the components superimposed at a specific m/z ratio versus their drift times through the IM cell; it can be displayed as a 2D map with ion intensities represented by color brightness or as a line plot (like an LC chromatogram) of ion intensity versus drift time (vide supra). Absolute ion intensities of the mobility-separated ions were extracted from the mobilograms by the MassLynx V4.1 software; from these, normalized relative abundances for the complexes participating in a fission–fusion equilibrium were calculated and plotted versus concentration to monitor the macromolecular interconversions taking place over the sampled concentration ranges. The MassLynx software used a peak picking and area calculation algorithm, with which the actual peaks present in the IM-MS mobilogram can be identified, and if needed deconvoluted, for the determination of relative proportions.

Experimental CCS values were derived from the drift times of the mobility-separated ions and theoretical CCSs of specific architectures were obtained by molecular modeling. The procedures for determining the experimental CCSs and calculating the theoretical CCSs of the assemblies studied here have been previously reported.<sup>[39,41]</sup>

## Supporting Information

Supporting Information is available from the Wiley Online Library or from the author.

## Acknowledgements

Funding from the National Science Foundation (CHE-1808115) is gratefully acknowledged.

## **Conflict of Interest**

The authors declare no conflict of interest.

## Keywords

equilibrium constants, fusion–fission equilibria, ion mobility-mass spectrometry, quantitative supramolecular mixture analysis, thermodynamic stabilities



www.advancedsciencenews.com

Macromolecular
Rapid Communications
www.mrc-journal.de

Received: September 7, 2018 Revised: November 2, 2018 Published online:

- [1] J. M. Berg, J. L. Tymoczko, G. J. GattoJr., L. Stryer, *Biochemistry*, 8th ed., W. H. Freeman and Co., New York **2015**.
- [2] V. M. Bolanos-Garcia, Q. Wu, T. Ochi, D. Y. Chirgadze, B. L. Sibanda, T. L. Blundell, *Philos. Trans. R. Soc.*, A 2012, 370, 3023.
- [3] H. Wu, Cell 2013, 153, 287.
- [4] B. J. G. E. Pieters, M. B. Eldijk, R. J. M. Nolte, J. Mecinović, Chem. Soc. Rev. 2016, 45, 24.
- [5] M. V. Shapovalov, Q. Wang, Q. Xu, M. Andrake, R. L. Dunbrack, PLoS One 2014, 9, e98309.
- [6] L. King, G. Weber, Biochemistry 1986, 25, 3637.
- [7] T. Ikkai, H. Kondo, J. Biochem. Biophys. Methods 1996, 33, 55.
- [8] P. Arosio, B. Jaquet, H. Wu, M. Morbidelli, *Biophys. Chem.* 2012, 168–169, 19.
- [9] J. Zhang, in Protein-Protein Interactions Computational and Experimental Tools (Ed: W. Cai), InTech, Rijeka, Croatia 2012, Ch. 18, p. 359.
- [10] V. Uversky, A. L. Fink (Eds.), Protein Misfolding, Aggregation, and Conformational Disease Part A: Protein Aggregation and Conformational Diseases, Springer Science, Singapore 2006.
- [11] S. E. Ahnert, J. A. Marsh, H. Hernández, C. V. Robinson, S. A. Teichmann, Science 2015, 350, aaa2245.
- [12] Y. Song, M. T. Nelp, V. Bandarian, V. H. Wysocki, ACS Cent. Sci. 2015. 1, 477.
- [13] C. S. Kaddis, J. A. Loo, Anal. Chem. 2007, 79, 1778.
- [14] D. E. Clemmer, S. J. Valentine, Nat. Chem. 2009, 1, 257.
- [15] C. R. Uetrecht, R. J. Rose, E. van Duijn, K. Lorenzen, A. J. R. Heck, Chem. Soc. Rev. 2010, 39, 1633.
- [16] M. T. Bowers, Int. J. Mass Spectrom. 2014, 370, 75.
- [17] J. D. Eschweiler, A. T. Frank, B. T. Ruotolo, J. Am. Soc. Mass Spectrom. 2017, 28, 1991.
- [18] T. Wyttenbach, J. Gidden, M. T. Bowers, in Ion Mobility Spectrometry-Mass Spectrometry (Eds: C. L. Wilkins, S. Trimpin), CRC Press, Boca Raton, FL 2010, Ch. 1, p. 3.
- [19] E. Jurneczko, P. E. Barran, Analyst 2011, 136, 20.
- [20] C. Wesdemiotis, Angew. Chem., Int. Ed. 2017, 56, 1452.
- [21] E. S. Baker, S. L. Bernstein, M. T. Bowers, J. Am. Soc. Mass Spectrom. 2005, 16, 989.
- [22] M. F. Jarrold, Phys. Chem. Chem. Phys. 2007, 9, 1659.
- [23] F. Albrieux, H. Ben Hamidane, F. Calvo, F. Chirot, Y. O. Tsybin, R. Antoine, J. Lemoine, P. Dugourd, J. Phys. Chem. A 2011, 115, 4711.
- [24] N. A. Pierson, L. Chen, D. H. Russell, D. E. Clemmer, J. Am. Chem. Soc. 2013, 135, 3186.
- [25] A. López, M. Vilaseca, S. Madurga, M. Varese, T. Tarragó, E. Giralt, J. Mass Spectrom. 2016, 51, 504.

- [26] S. Poyer, C. Comby-Zerbino, C. M. Choi, L. MacAleese, C. Deo, N. Bogliotti, J. Xie, J. Y. Salpin, P. Dugourd, F. Chirot, *Anal. Chem.* 2017, 89, 4230.
- [27] T. Aida, E. W. Meijer, S. I. Stupp, Science 2012, 335, 813.
- [28] T. R. Cook, Y.-R. Zheng, P. J. Stang, Chem. Rev. 2013, 113, 734.
- [29] A. Winter, U. S. Schubert, Chem. Soc. Rev. 2016, 45, 5311.
- [30] S. Chakraborty, G. R. Newkome, Chem. Soc. Rev. 2018, 47, 3991.
- [31] U. S. Schubert, A. Winter, G. R. Newkome, Terpyridine-Based Materials: For Catalytic, Optoelectronic and Life Science Applications, Wiley-VCH, Weinheim, Germany 2011.
- [32] Y.-T. Chan, X. Li, G. A. Carri, C. N. Moorefield, G. R. Newkome, C. Wesdemiotis, J. Am. Chem. Soc. 2011, 133, 11967.
- [33] K. Guo, Z. Guo, J. M. LudlowIII, T. Xie, S. Liao, G. R. Newkome, C. Wesdemiotis, Macromol. Rapid Commun. 2015, 36, 1539.
- [34] T.-Z. Xie, S.-Y. Liao, K. Guo, X. Lu, X. Dong, M. Huang, C. N. Moorefield, S. Z. D. Cheng, X. Liu, C. Wesdemiotis, G. R. Newkome, J. Am. Chem. Soc. 2014, 136, 8165.
- [35] S. Chakraborty, W. Hong, K. Endres, T.-Z. Xie, L. Wojtas, C. N. Moorefield, C. Wesdemiotis, G. R. Newkome, J. Am. Chem. Soc. 2017, 139, 3012.
- [36] X. Lu, X. Li, K. Guo, J. Wang, M. Huang, J.-L. Wang, T.-Z. Xie, C. N. Moorefield, S. Z. D. Cheng, C. Wesdemiotis, G. R. Newkome, *Chem. - Eur. J.* 2014, 20, 13094.
- [37] X. Lu, X. Li, K. Guo, T.-Z. Xie, C. N. Moorefield, C. Wesdemiotis, G. R. Newkome, J. Am. Chem. Soc. 2014, 136, 18149.
- [38] T.-Z. Xie, K. Guo, Z. Guo, W.-Y. Gao, L. Wojtas, G.-H. Ning, M. Huang, X. Lu, J.-Y. Li, S.-Y. Liao, Y.-S. Chen, C. N. Moorefield, M. J. Saunders, S. Z. D. Cheng, C. Wesdemiotis, G. R. Newkome, Angew. Chem., Int. Ed. 2015, 54, 9224.
- [39] T.-Z. Xie, K. J. Endres, Z. Guo, J. M. LudlowIII, C. N. Moorefield, M. J. Saunders, C. Wesdemiotis, G. R. Newkome, J. Am. Chem. Soc. 2016, 138, 12344.
- [40] J. M. Ludlowlll, M. Tominaga, Y. Chujo, A. Schultz, X. Lu, T. Xie, K. Guo, C. N. Moorefield, C. Wesdemiotis, G. R. Newkome, *Dalton Trans.* 2014, 43, 9604.
- [41] S. Chakraborty, K. J. Endres, R. Bera, L. Wojtas, C. N. Moorefield, M. J. Saunders, N. Das, C. Wesdemiotis, G. R. Newkome, *Dalton Trans.* 2018, 47, 7528.
- [42] M. A. R. Meier, B. G. G. Lohmeijer, U. S. Schubert, J. Mass Spectrom. 2003, 38, 510.
- [43] R. Dobrawa, P. Ballester, C. R. Saha-Möller, F. Würthner, in Metal-Containing and Metallomacromolecular Polymers and Materials (Ed: U. S. Schubert, G. R. Newkome, I. Manners), ACS Symposium Series 928, American Chemical Society, Washington, DC 2006, p. 43
- [44] G. Westmacott, M. Frank, S. E. Labov, W. H. Benner, Rapid Commun. Mass Spectrom. 2000, 14, 1854.
- [45] R. Liu, Q. Li, L. M. Smith, J. Am. Soc. Mass Spectrom. 2014, 25, 1374.